

# Enhanced Second Harmonic Generation from Coupled Asymmetric Plasmonic Metal Nanostructures

Bilge Can Yildiz,<sup>1,2,3</sup> Mehmet Emre Tasgin,<sup>4</sup> Musa Kurtulus Abak,<sup>5,2</sup>  
Sahin Coskun,<sup>6,2</sup> Husnu Emrah Unalan,<sup>6,5,2</sup> and Alpan Bek<sup>1,5,2</sup>

<sup>1</sup>*Department of Physics, Middle East Technical University, 06800, Ankara, Turkey*

<sup>2</sup>*The Center for Solar Energy Research and Applications (GUNAM),  
Middle East Technical University, 06800, Ankara, Turkey*

<sup>3</sup>*Physics Unit, Atılım University, 06836 Ankara, Turkey*

<sup>4</sup>*Institute of Nuclear Sciences, Hacettepe University, 06532, Ankara, Turkey*

<sup>5</sup>*Micro and Nanotechnology Program of Graduate School of Natural and Applied Sciences,  
Middle East Technical University, Ankara 06800, Turkey*

<sup>6</sup>*Department of Metallurgical and Materials Engineering,  
Middle East Technical University, 06800 Ankara, Turkey*

(Dated: May 9, 2022)

We show that second harmonic generation can be enhanced by Fano resonant coupling of asymmetric plasmonic metal nanostructures. We develop a theoretical model examining the effects of electromagnetic interaction between two metal nanostructures on the second harmonic generation. We compare the second harmonic generation efficiency of a single plasmonic metal nanostructure with that of two coupled ones. We show that second harmonic generation from a single metal nanostructure can be enhanced about 30 times by attaching a second metal nanostructure with a 10 times higher quality factor than that of the first one. The origin of this enhancement is Fano resonant coupling of the two metal nanostructures. We support our findings on Fano enhancement of second harmonic generation by an experimental study of a coupled plasmonic system composed of a silver nanoparticle and a silver nanowire on glass surface in which the ratio of the quality factors are also estimated to be around 10 times.

Keywords: Fano resonance, second harmonic generation, plasmons, nonlinear optics, enhancement

## I. INTRODUCTION

Typically, nonlinear optical effects appear at very high intensities, that is, nonlinear optical properties of material surfaces can only be revealed by pulsed lasers. In recent studies [1, 2], material surfaces or interfaces decorated with metal nanostructures are suggested to act as nonlinear conversion agents as they are considered to. This property is expected to enable these efficient nonlinear converters to be utilized in many application areas, such as solar energy, molecular switching, photocatalysis, imaging, etc.

When a quantum dot with a sharp resonance is attached to a metal nanostructure (MNS), a dip in the absorption spectrum of the MNS is observed. Such transparencies are called Fano resonances [3] and are introduced due to out-of-phase absorption through hybridized excitation paths [4]. Such resonances in the plasmonic response of MNSs are responsible for increased fluorescence of molecules [5] and increased lifetime of plasmonic oscillations [6] which makes coherent plasmon emission possible [7, 8].

Plasmon oscillations in MNSs concentrate the incident light to nm dimensions which yield strong enhancement in the field intensities [8]. The enhancement in the intensity leads to the appearance of optical nonlinearities such as enhanced Raman scattering [9], four wave mixing [10], and second harmonic generation (SHG) [11–16]. Fano resonances with attached quantum objects can be utilized to enhance [11] and suppress [1] the SHG pro-

cess in plasmonic particles. The underlying mechanism relies on the cancellation of nonresonant frequency terms degrading the frequency conversion by hybridized paths [1].

Fano-like resonances can also take place in two coupled classical oscillators [4, 17], without quantum nature. It is also experimentally demonstrated that coupling with dark modes (which have longer lifetimes) [18, 19] can result in Fano resonances.

In this paper, we address the question if SHG from two coupled oscillators (that is two coupled MNSs) can also be enhanced or suppressed by utilizing the fully classical Fano resonances [4, 17–19]. We show both experimentally and theoretically that SHG enhancement in hybrid structures can be obtained even in the absence of coupled quantum oscillators. This is an important simplification for facilitating the use of purely metal nanostructures with appropriate experimental function. By the use of carefully designed metal nanostructures, enhanced nonlinear conversion of light can be achieved. In this paper we demonstrate theoretically that the second harmonic generation can be enhanced by systems of coupled MNSs. We support our theoretical model and Fano enhancement findings by an experimental study in which we construct a coupled MNS system composed of a silver nanoparticle (AgNP) of  $\sim 100$  nm size and a silver nanowire (AgNW) of  $\sim 60$  nm diameter and several microns length on a dielectric (glass) surface. When a 1064 nm infrared (IR) excitation laser is focused solely on AgNW, a weak 532 nm SHG signal is generated. Strikingly, as the focus is

moved along the AgNW axis, it is found that the generated SHG signal is enhanced by up to a factor of 30 when the focus is in the vicinity of AgNP coupled region. The observed enhancement factor of  $\sim 30$  is in a very good agreement with the prediction value of 32 from the presented theoretical model.

## II. THEORETICAL MODEL

In this section, we develop a theoretical model describing the second harmonic response of a system of two coupled plasmonic oscillators. We introduce the effective Hamiltonian for the system and derive the equations of motion for the plasmon-polariton mode fields. We numerically time evolve the equations to obtain the steady state occupations of the plasmon modes and show that second harmonic conversion generation can be either enhanced or suppressed by choosing an appropriate MNS supporting a particular frequency mode.

We treat the MNSs as if they do not have a spatial extent, i.e. they are point particles. In the physical situation, however, the particles must have sizes and hence there must be retardation effects. In ref. [1], coupling of a MNS and a quantum emitter object is treated with the same theoretical model. It is shown that the simple model can well predict the amount and the spectral position of the SHG enhancement by comparing the results with the simulations performed by using MNPBEM Toolbox in MATLAB [20]. The simulations take the retardation effects into account, the physical objects are simulated with their true geometries.

### A. The model system

We consider two MNSs which support plasmonic excitations at optical wavelengths. The MNSs interact with each other due to induced charge oscillations. The first MNS supports two plasmon modes of resonances  $\omega_1$  and  $\omega_2$ , see Fig. 1b solid yellow curve. Shape of the second MNS is chosen so that it has a single plasmonic response peaked at  $\omega_b$ , see Fig. 1b dashed green curve, in the relevant frequency region.

The first MNS has non-centrosymmetric shape (the spherical shape in Fig. 1a is for demonstrative purposes), so it can perform second harmonic (SH) frequency conversion. The lower energetic mode ( $\omega_1$ ) of the first MNS is driven resonantly by an external harmonic electromagnetic field of frequency  $\omega$ . The frequencies of the plasmon modes of the first MNS are chosen so that the resonant SH conversion condition ( $\omega_2 \approx 2\omega$ ) is satisfied. The resonance peak of the second MNS is chosen to vary around  $\omega_1$  and  $\omega_2$ . Both modes of the first MNS couples with the  $\omega_b$  oscillations.

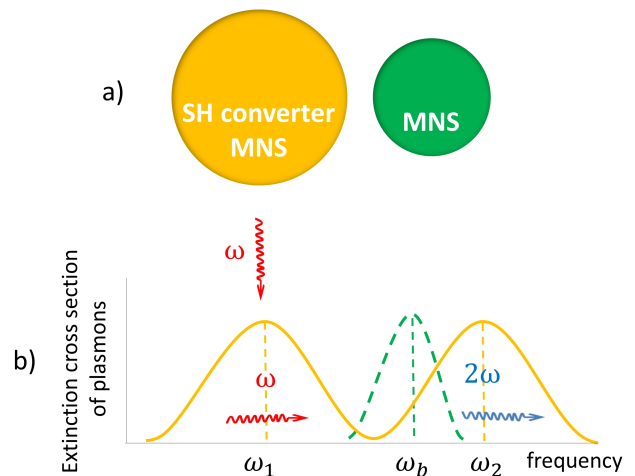


FIG. 1: A representative picture of the coupled oscillators, and their resonances. First oscillator supports two modes,  $\omega_1$  and  $\omega_2$ , where the two frequencies are approximately equal to the driving and second harmonic field frequencies respectively. Second oscillator is coupled with the first oscillator hereby effecting the second harmonic generation process.

### B. Hamiltonian

Dynamics of the system is as follows. An incident planewave radiation,  $\varepsilon_p e^{-i\omega t}$ , drives the first mode,  $\omega_1$ , of the first (SH converter) MNS and induces plasmonic excitations oscillating at frequency  $\omega$ . The polarization of the plasmon-polariton (PP) excitation yields a localized strong electromagnetic field mode ( $\hat{a}_1$ ) in the plasmonic structure. This localized strong field enables multiphoton (plasmon) processes come into play. The field oscillating at frequency  $\omega$  trapped in the  $\omega_1$  PP polarization gives rise to the second harmonic polarization oscillations at  $2\omega$  in the  $\omega_2$  mode.  $\omega_b$  mode of the second MNS interacts with both  $\omega_1$  and  $\omega_2$  modes. The interaction strengths can be tuned either by varying  $\omega_b$  or by changing the position or shape of the second MNS (i.e. changing the overlap integral).

The total Hamiltonian can be written as the sum of the energies of the plasmons in the first ( $\hat{H}_a$ ) and the second ( $\hat{H}_b$ ) MNSs, the interaction between the MNSs ( $\hat{H}_{int}$ ), the energy supplied by the incident field ( $\hat{H}_p$ ), and the term governing the second harmonic generation process ( $\hat{H}_{sh}$ ),

$$\hat{H} = \hat{H}_a + \hat{H}_b + \hat{H}_{int} + \hat{H}_p + \hat{H}_{sh}. \quad (1)$$

where

$$\hat{H}_a = \hbar\omega_1 \hat{a}_1^\dagger \hat{a}_1 + \hbar\omega_2 \hat{a}_2^\dagger \hat{a}_2, \quad (2)$$

$$\hat{H}_b = \hbar\omega_b \hat{b}^\dagger \hat{b}, \quad (3)$$

$$\hat{H}_{int} = \hbar(f_1 \hat{a}_1^\dagger \hat{b} + f_1^* \hat{a}_1 \hat{b}^\dagger) + \hbar(f_2 \hat{a}_2^\dagger \hat{b} + f_2^* \hat{a}_2 \hat{b}^\dagger), \quad (4)$$

$$\hat{H}_p = i\hbar(\hat{a}_1^\dagger \epsilon_p e^{-i\omega t} - \hat{a}_1 \epsilon_p^* e^{i\omega t}), \quad (5)$$

$$\hat{H}_{sh} = \hbar\chi^{(2)}(\hat{a}_2^\dagger \hat{a}_1 \hat{a}_1 + \hat{a}_1^\dagger \hat{a}_1^\dagger \hat{a}_2). \quad (6)$$

$\hat{a}_1$  and  $\hat{a}_2$  are the annihilation operators for the collective plasmon excitations in the first MNS, corresponding to the modes with resonance frequencies  $\omega_1$  and  $\omega_2$  respectively. Similarly,  $\hat{b}$  is the annihilation operator for  $\omega_b$  mode of the second MNS. ( $\hat{a}_1$ ,  $\hat{a}_2$  and  $\hat{b}$  will represent the amplitudes of the related plasmon oscillations.)  $f_1$  ( $f_2$ ) is the coupling matrix element between the field induced by  $\hat{a}_1$  ( $\hat{a}_2$ ) mode of the SH converter (first MNS) and the  $\hat{b}$  mode of the second MNS. Eq. (5) describes the interaction of the incident field which drives  $\hat{a}_1$  PP mode. Eq. (6), two low energetic plasmons in  $\hat{a}_1$  mode oscillating at  $\omega$ , combine to generate a second harmonic plasmon in  $\hat{a}_2$  mode, oscillating at  $2\omega$ . The parameter  $\chi^{(2)}$ , in units of frequency, is proportional to the second harmonic susceptibility of the oscillator.

We use Heisenberg equation of motion,  $i\hbar\dot{\hat{A}} = [\hat{A}, \hat{H}]$  for any operator  $\hat{A}$ , to derive the time evolution of the plasmon amplitudes. After obtaining the quantum dynamics of each mode, since we are not interested in the entanglement features but only in intensities, we substitute the quantum operators  $\hat{a}_1$ ,  $\hat{a}_2$ , and  $\hat{b}$  with their expectation values,  $\alpha_1$ ,  $\alpha_2$ , and  $\alpha_b$ . We plug in the damping rates for the PP fields, namely  $\gamma_1$ ,  $\gamma_2$ , and  $\gamma_b$  respectively. Consequently we obtain the following equations for the plasmon amplitudes.

$$\dot{\alpha}_1 = (-i\omega_1 - \gamma_1)\alpha_1 - f_1\alpha_b + \epsilon_p e^{-i\omega t} - 2i\chi^{(2)}\alpha_1^* \alpha_2 \quad (7)$$

$$\dot{\alpha}_2 = (-i\omega_2 - \gamma_2)\alpha_2 - f_2\alpha_b + i\chi^{(2)}\alpha_1^2 \quad (8)$$

$$\dot{\alpha}_b = (-i\omega_b - \gamma_b)\alpha_b - f_1\alpha_1 - if_2\alpha_2 \quad (9)$$

In the steady state, the oscillation modes can only support the driving frequency ( $\omega$ ) and the SH generated frequency ( $2\omega$ ) of the form

$$\alpha_1 = \alpha_1^{(1)} e^{-i\omega t} + \alpha_1^{(2)} e^{-i2\omega t}, \quad (10)$$

$$\alpha_2 = \alpha_2^{(1)} e^{-i\omega t} + \alpha_2^{(2)} e^{-i2\omega t}, \quad (11)$$

$$\alpha_b = \alpha_b^{(1)} e^{-i\omega t} + \alpha_b^{(2)} e^{-i2\omega t}. \quad (12)$$

Amplitudes  $\alpha_1^{(1)}$ ,  $\alpha_2^{(1)}$  and  $\alpha_b^{(1)}$  are the amplitudes of linear plasmon oscillations ( $\omega$ ), and  $\alpha_1^{(2)}$ ,  $\alpha_2^{(2)}$  and  $\alpha_b^{(2)}$  are the amplitudes of the second harmonic ( $2\omega$ ) plasmon oscillations.

We numerically time evolve equations (7,8,9) and then obtain the time behaviour after steady state has been reached. Using the Fourier transform technique we determine the steady state amplitudes,  $\alpha_1^{(2)}$ ,  $\alpha_2^{(2)}$  and  $\alpha_b^{(2)}$ , exhibiting the amplitudes of second harmonic oscillations. The number of SH plasmons can be determined by summing over the plasmons generated in all three modes as

$$N_{sh} \equiv |\alpha_1^{(2)}|^2 + |\alpha_2^{(2)}|^2 + |\alpha_b^{(2)}|^2. \quad (13)$$

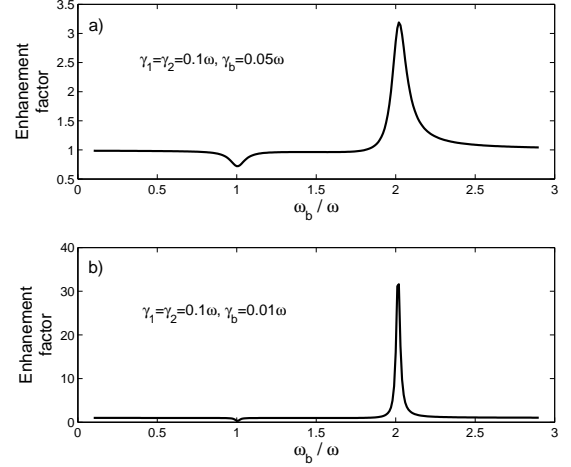


FIG. 2: Enhancement factor with changing resonance frequency of the second MNS,  $\omega_b$  for the coupling of the MNSs with decay rates, a)  $\gamma_1 = \gamma_2 = 0.1\omega$  and  $\gamma_b = 0.05\omega$ , b)  $\gamma_1 = \gamma_2 = 0.1\omega$  and  $\gamma_b = 0.01\omega$ .

We note that  $e^{-i2\omega t}$  oscillations in  $\alpha_1$  and  $\alpha_b$  modes are not generated in these modes. They are rather transferred from  $\alpha_2$  mode due to interactions.

### C. Tuning the second harmonic conversion

We are interested in the enhancement and suppression of the SHG from the first MNS, in the presence of alternative absorption/emission paths due to the coupling with the second MNS. We compare the number of  $2\omega$  plasmons generated in the presence of coupling ( $f_1 \neq 0, f_2 \neq 0$ ),  $N_{sh}$ , to the number of  $2\omega$  plasmons in the absence of coupling ( $f_1 = 0, f_2 = 0$ ),  $N_{sh}^{(0)}$ . Thus, we define the enhancement factor as the ratio of  $N_{sh}$  to  $N_{sh}^{(0)}$ .

$$\text{Enhancement factor} \equiv \frac{N_{sh}}{N_{sh}^{(0)}} \quad (14)$$

In order to identify the spectral positions of the nonlinear Fano resonances, we calculate the SHG enhancement factor for different resonance frequencies,  $\omega_b$ , of the second MNS. In our simulations, we fix the parameters

$\omega_1 = \omega$ ,  $\omega_2 = 2\omega$ ,  $\gamma_1 = \gamma_2 = 0.1\omega$ ,  $f_1 = 0.2\omega$  and  $f_2 = 0.8\omega$ . In Figs 2a and 2b, we set the decay rate of the second MNS as  $\gamma_b = 0.05\omega$  and  $\gamma_b = 0.01\omega$ , respectively.

Fig. 2a, where  $\gamma_b = 0.05\omega$ , shows that in the case of two coupled MNS, SHG can be enhanced more than three times as compared to the case of the first MNS alone. Maximum enhancement is obtained when the resonance of the second MNS is tuned to  $\omega_b = 2.02\omega$ . On the contrary, SHG can be suppressed to 0.72 when  $\omega_b$  is tuned to  $\omega_b = 1\omega$ . Fig. 2b shows that when a second MNS with smaller damping ( $\gamma_b = 0.01\omega$ ) is used, a smaller suppression but much larger enhancement can be obtained. At  $\omega_b = 2.02\omega$  ( $\omega_b = 1\omega$ ), enhancement (suppression) factor of 32 (0.31) is found.

Emergence of enhancement at about  $\omega_b \approx 2\omega$  can be understood using the arguments given in ref. [1]. The off-frequency term that is  $\omega_2 - 2\omega$  is cancelled by an auxiliary term which emerges due to the path interference effects (see the discussion below Eq. (9) in ref. [1]). Suppression at  $\omega_b = 1\omega$  take place since the linear path interference does not allow the excitation at the driving frequency  $\omega$ . When the linear response is suppressed, smaller  $\omega$  ( $\hat{a}_1$ ) plasmon intensities result in less SH conversion.

In the following section, we report the results of the experiment of a silver nanowire- silver nanoparticle system locally illuminated with a Gaussian beam source.

### III. EXPERIMENT

In this section we explain the details of the experimental study on a similar system to the one studied within the theoretical model, a system of two coupled plasmonic oscillators; a silver nanowire and a silver nanoparticle.

#### A. Colloidal solution preparation procedure

Silver nanowires are synthesized by self-seeding polyol process. In this technique, an inorganic salt is reduced by a polyol and agglomeration of particles is prevented by addition of surfactant which is commonly polyvinylpyrrolidone (PVP). Required chemicals are bought from Sigma-Aldrich. 7 mg of NaCl is added into 10 mL of 0.45 M ethylene glycol (EG) solution of PVP and heated at 170°C. By using injection pump, solution of 0.12 M AgNO<sub>3</sub> in 5 mL of EG is added dropwise at a rate of 5 mL/h. During this process, solution is stirred at 1000 rpm rate by magnetic stirrer. After the drop-wise EG addition process, solution is heated up at 170°C for 30 minutes and is cooled to room temperature. To enable the removal of polymer from the solution, the diluted solution with acetone is centrifuged two times for 20 minutes at 6000 rpm. Afterwards, wires are dispersed in ethanol and centrifuged again under the same conditions. At the end of this procedure, nanowires with 60 nm diameter and length of 8 to 10  $\mu\text{m}$  are obtained.

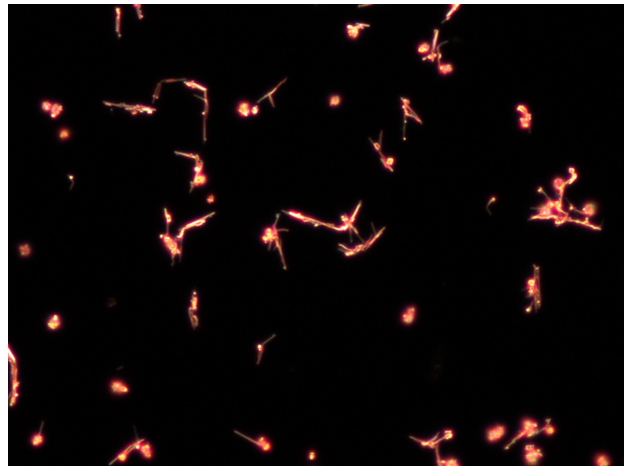


FIG. 3: A darkfield image of the AgNW - AgNP network deposited on microscope cover-slip. Light colored long straight features in the image represent the AgNWs and the bright intense spots represent the AgNPs.

Synthesis of silver nanospheres are carried out with a modified procedure of wire synthesis without addition of NaCl and silver nanospheres of around 100 nm diameter are acquired [21]. Solution containing bipyramids of metallic silver is synthesized with polymer-mediated polyol process as well. 94 mM AgNO<sub>3</sub> is added to 3 mL EG solution. Another 3 mL of EG solution containing 0.11 mM NaBr and 144 mM PVP is prepared and two solutions are added dropwise into heated EG solution of 5 mL in an oil bath at 160°C which contains 30  $\mu\text{L}$  of 10 mM NaBr. After 5 hours, bipyramid solution with an average size of 150 nm is obtained [21, 22].

The resulting AgNPs are co-deposited on the same substrates of AgNWs to obtain a network of NW-NP complexes, which are ultimately asymmetric structures and cover a macroscopically large area. Such coated surfaces are first imaged by dark-field microscopy to ensure the existence of the complexes (Fig. 3). The AgNPs are observed to display different colors such as green and blue under white light illumination as a result of their size dependent plasmon resonance in the visible range. The AgNWs are observed to show a reddish glimmer as a result of shift of their plasmon resonance towards IR due to high aspect ratio of their geometry. A combination of such two Ag nanostructures is what we expect to boost the SHG due to conversion of IR plasmons to visible plasmons upon interaction of NWs with NPs.

Next we place such a sample under our other optical setup with the piezo-stage.

#### B. Optical measurement

We used an inverted microscope (Zeiss model Axiovert 200) with a 63X (1.4 NA) objective lens for our experiments. In Fig. 4, a scheme of experimental setup is

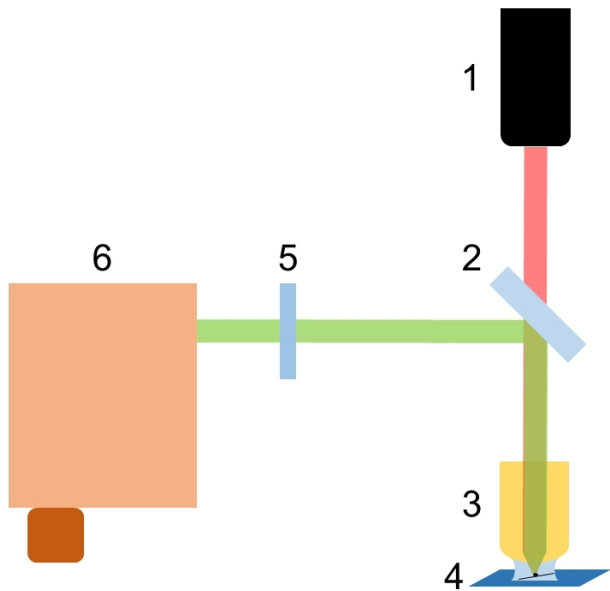


FIG. 4: The experimental setup: 1- cw Nd:YAG laser with  $\lambda = 1064$  nm, 2- long-pass dichroic mirror, 3- microscope objective, 4- sample, 5- short-pass filter (cut-off at 800 nm), 6- monochromator with CCD camera

displayed. We used a cw Nd:YAG laser (Cobolt model Rumba) with wavelength of  $\lambda = 1064$  nm and 500 mW output power as excitation source. The IR signal was delivered from the back port of microscope, resulting in an intensity of  $40 \text{ MW/cm}^2$  on the sample. Resulting SHG from the AgNW-AgNP cluster was registered by a spectrometer (Andor models Shamrock 750 spectrograph + Newton 971 EMCCD) in corporation with a long-pass dichroic mirror cutting off the backscattered 1064 nm signal and reflecting a band of 520-750 nm.

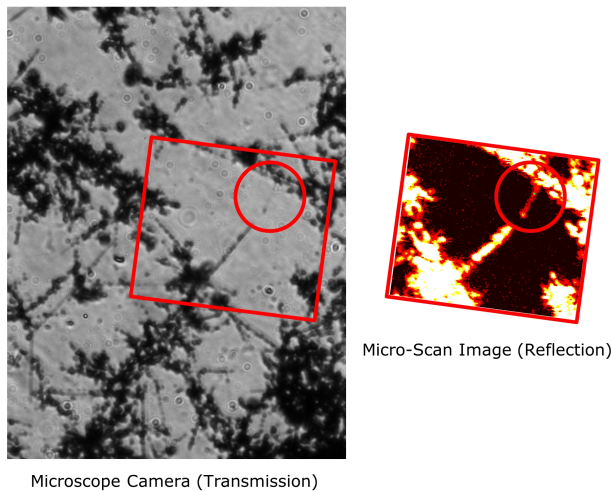


FIG. 5: A transmission image by the microscope camera on the left and a micro-scan reflection image of the area as indicated by the red rectangle, on the right. The red circles show a region with a single AgNW with a single AgNP attached close to its end.

We first record a transmission image by the visual inspection camera that works in the visible, see Fig. 5. The dark figures in the image indicate the location of AgNWs, AgNPs and their clusters with a very poor resolution. Nevertheless this image is sufficient to locate a candidate region that bears a single AgNW-AgNP complex for further detailed study. The red circle on the transmission image on the left points a region of possible interest with one NW and NP complex. The red rectangle indicates the region which is scanned at a high resolution by the piezo-stage. The reflection image produced by the scanning of the same region is given on the right using a 1064 nm IR laser. The reflection image produced at the illumination wavelength shows intense reflection from crowded clusters as well as a single straight feature which is the isolated part of a single AgNW and an AgNP attached towards the end of the AgNW. The faint straight shadow on the left image and a dark spot at its end appear as a straight bright feature on the left with a brighter spot at its end that indicates the attached AgNP.

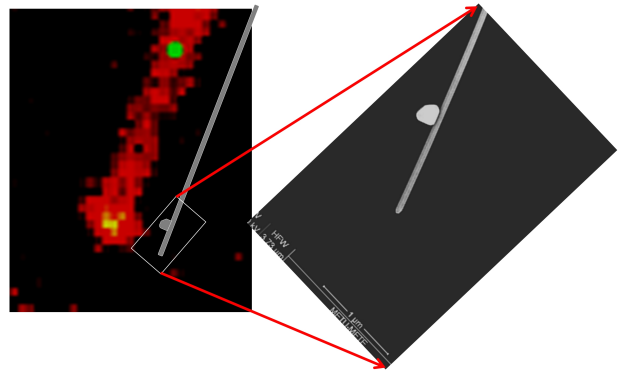


FIG. 6: A zoom in into the encircled region in the micro-scan image along with a sketch of AgNW-AgNP complex. The SEM image on the right shows the end of the AgNW with high magnification.

Such AgNW-AgNP complexes are often encountered upon inspection of these samples with scanning electron microscope. Fig. 6 shows a zoomed version of the encircled straight part of the micro-scan image along with a representative sketch of the AgNW-AgNP complex drawn to scale. An SEM image is provided on the right that shows a highly magnified image of the end of AgNW with the attached AgNP along its body. The AgNW is typically of 50-60 nm in diameter and can be as long as 5-10  $\mu\text{m}$ . The AgNPs are typically of 50-150 nm size.

### C. Experimental results

By the help of the micro-scan image, we can direct our focal spot at any pixel of choice and acquire SHG spectra using a spectrometer EMCCD combination (see the green points in the image frames in Fig. 7). In Fig. 7

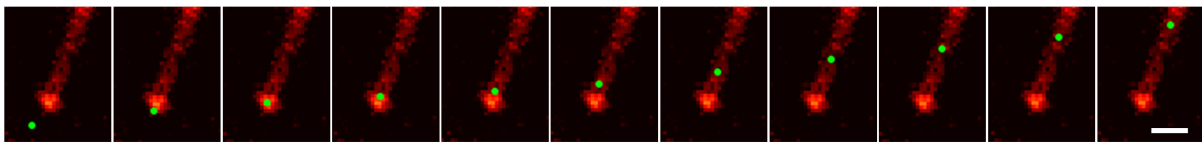


FIG. 7: A series of IR micro-scan images with green markings showing selected illumination spots. The white scale bar represents  $2 \mu\text{m}$ . The green points span a total of about  $6 \mu\text{m}$  distance.

we show a series of frames on which the particular choice of illumination spots are marked and at those positions SHG spectra around  $532 \text{ nm}$  of SHG wavelength are accumulated. While moving the diffraction limited illumination spot along the axis of the AgNW, a SHG spectrum is acquired at each indicated green spot from left to right and the acquired spectra are plotted (Fig. 8 inset). These spectra are integrated and the integral SHG signal is plotted against the distance along the AgNW axis (Fig. 8).

There are 3 major results that we obtain. 1) When the illumination spot is not located on the AgNW, no SHG signal is registered. So the SHG originates genuinely from the plasmonic structure. 2) We observe SHG even with cw illumination ( $50 \text{ mW}$  on the sample) from AgNW plasmonic structures. 3) The SHG signal is enhanced by a factor of about 30 when the illumination spot is on the AgNP-AgNW complex with respect to the body of the AgNW alone.

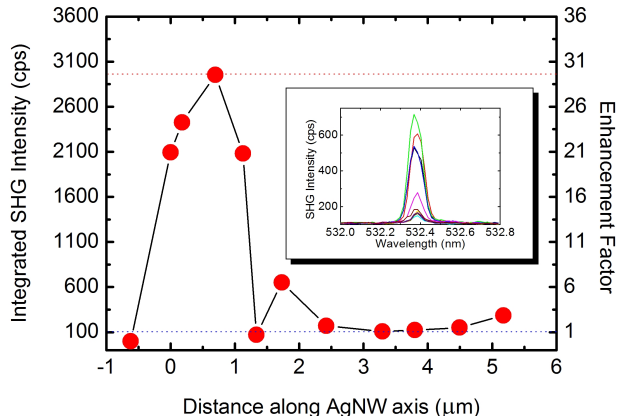


FIG. 8: The SHG spectra obtained at different positions along the body of the AgNW (inset). The integrated SHG intensity (left vertical axis) and the enhancement factor (right vertical axis) as a function of position on the AgNW. The breadth of the SHG signal peak along the AgNW axis is due to the  $1 \mu\text{m}$  focal spot size.

A better visual representation of the SHG intensity distribution as a function of position along the AgNW axis is given in Fig. 9. A color bar is produced from the integral SHG signal and displayed in parallel with the actual SEM image and its representative straight extension. The SHG signal clearly appears starting from the end of the AgNW and reaches its maximum around where the

AgNP is attached to the AgNW. An overlap of the color bar with a representation of such an AgNW-AgNP plasmonic hybrid complex on the right clearly depicts the observed effect: An effective SHG conversion spot is constructed by the hybridization of the AgNW and AgNP plasmons.

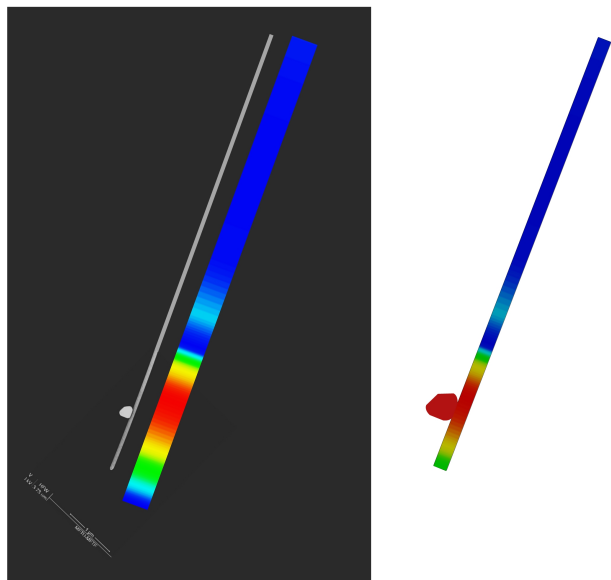


FIG. 9: The SHG integral signal intensity as a color bar and the AgNW along with it, clearly show that the enhancement originates from coupling of the AgNW with the AgNP. The color bar superposed onto the representative sketch of the system - on the right.

#### IV. DISCUSSION AND CONCLUSIONS

In this paper we study the tunability of SHG from a coupled system of metal nano particle and a nanowire. Our experiments show that SHG from nanoparticles or nanowires can be enhanced about 30 times as compared to the uncoupled ones, by utilizing the path interference effects. We also introduce a single theoretical model and demonstrate the origin of the enhancement in our experiment.

Silver nanoparticle and nanowire samples are illuminated with continuous wave IR laser source of  $1064 \text{ nm}$  wavelength at different focal points with a focal spot size

1  $\mu\text{m}$  diameter. First, AgNW and AgNP samples of typical sizes 5  $\mu\text{m}$  and 100 nm respectively, are illuminated separately and SH response is recorded. Second, the two MNSs are combined and a representative coupled MNS is identified. The focus of IR laser is moved stepwise along the axis and the SH response at 532 nm wavelength is recorded at each step (Fig. 8). It is observed that when the laser focus is in the region containing the coupled AgNP, the SH signal is enhanced up to 30 times as compared to the AgNP-free regions on AgNW axis.

Our experimental results can be interpreted by help of the developed theoretical model examining the effects of coupling of a MNS with a SH converter MNS. We show that the enhancement factor ( $\sim 30$ ) observed in the experiment can be obtained by attaching a higher quality MNS to the SH converter MNS. The attached MNS has a distorted bipyramidal shape and can support dark modes with relatively longer lifetimes than that of bright modes. Therefore in our experiment AgNW plays the role of SH converter and bipyramid AgNP is the coupled higher quality plasmonic oscillator. This is also confirmed by control experiments performed on AgNW and AgNP samples separately, where the former is found to generate  $\sim 6$  times higher SH conversion.

Alzar et. al. show that absorption cancellations due to Fano resonances can be achieved in entirely classical

systems [4]. In this work, we demonstrate both experimentally and theoretically that Fano resonances can also give rise to enhancement of nonlinear responses in entirely classical systems. Hence, nonlinear enhancement by Fano resonances does not necessarily take place only in coupled classical-quantum systems [1, 2].

### Acknowledgements

The research leading to these results has received funding from: the European Union's Seventh Framework Programme FP7/2007-2013 under grant agreement nr. 270483; and Bilim Akademisi - The Science Academy, Turkey under the BAGEP program (A.B.). A.B. acknowledges support from TUBITAK Grants No. 113F239, 113M931, 113F375 and 114E105. M.E.T. acknowledges support from TUBITAK Grants No. 112T927 and No. 114F170. We would like to thank Dr. Marco Lazzarino and Dr. Denys Naumenko from Laboratorio TASC, CNR-IOM for useful discussions and help with the experiments. We also thank Dr. Oguz Gulseren from Bilkent University, Ankara, Turkey for his support.

- 
- [1] D. Turkpence, M. E. Tasgin, G. B. Akguc, A. Bek, Engineering nonlinear response of nanomaterials using fano resonances., *Journal of Optics* 16 (10) (2014) 105009 (10pp).
- [2] I. Salakhutdinov, D. Kendziora, M. K. Abak, D. Turkpence, L. Piantanida, L. Fruk, M. E. Tasgin, M. Lazzarino, A. Bek, Plasmonic non-linear conversion of continuous wave light by gold nanoparticle clusters with fluorescent protein loaded gaps. arXiv:1402.5244v2 (2014).
- [3] A. E. Miroshnichenko, Y. S. Kivshar, S. Flach, Fano resonances in nanoscale structures., *Reviews of Modern Physics* 82 (3) (2010) 2257–2298.
- [4] C. L. G. Alzar, M. A. G. Martinez, P. Nussenzveig, Classical analog of electromagnetically induced transparency., *American Journal of Physics* (1) (2002) 37.
- [5] C. Ayala-Orozco, J. G. Liu, M. W. Knight, Y. Wang, J. K. Day, P. Nordlander, N. J. Halas, Fluorescence enhancement of molecules inside a gold nanomatryoshka., *Nano Letters* 14 (5) (2014) 2926 – 2933.
- [6] M. E. Tasgin, Metal nanoparticle plasmons operating within a quantum lifetime., *Nanoscale* 5 (18) (2013) 8616 – 8624.
- [7] M. A. Noginov, G. Zhu, A. M. Belgrave, S. Stout, R. Bakker, V. M. Shalaev, E. E. Narimanov, E. Herz, T. Suteewong, U. Wiesner, Demonstration of a spaser-based nanolaser., *Nature* 460 (7259) (2009) 1110–1112.
- [8] M. I. Stockman, Nanoplasmonics: Past, present, and glimpse into future., *Optics Express* 19 (22) (2011) 22029–22106.
- [9] B. Sharma, R. R. Frontiera, A.-I. Henry, E. Ringe, R. P. Van Duyne, Sers: Materials, applications, and the future., *Materials Today* 15 (1-2) (2012) 16.
- [10] P. Genevet, J. P. Tetienne, M. A. Blanchard, R. and Kats, F. Capasso, E. Gatzogiannis, M. O. Scully, Large enhancement of nonlinear optical phenomena by plasmonic nanocavity gratings., *Nano Letters* 10 (12) (2010) 4880–4883.
- [11] K. Thyagarajan, J. Butet, O. J. F. Martin, Augmenting second harmonic generation using fano resonances in plasmonic systems., *Nano Letters* 13 (4) (2013) 1847–1851.
- [12] J. Berthelot, M. Song, P. Rai, G. C. Des Francs, A. Dereux, A. Bouhelier, G. Bachelier, Silencing and enhancement of second-harmonic generation in optical gap antennas., *Optics Express* 20 (10) (2012) 10498–10508.
- [13] S. Wunderlich, U. Peschel, Plasmonic enhancement of second harmonic generation on metal coated nanoparticles., *Optics Express* 21 (16) (2013) 18611 – 18623.
- [14] S. Gao, K. Ueno, H. Misawa, Plasmonic antenna effects on photochemical reactions., *Accounts of Chemical Research* 44 (4) (2011) 251–260.
- [15] M. R. Singh, Enhancement of the second-harmonic generation in a quantum dot-metallic nanoparticle hybrid system., *Nanotechnology* 24 (12) (2013) 125701 – 125706.
- [16] G. F. Walsh, L. Dal Negro, Enhanced second harmonic generation by photonic-plasmonic fano-type coupling in nanoplasmonic arrays., *Nano Letters* 13 (7) (2013) 3111 (6pp).
- [17] P. Tassin, L. Zhang, R. Zhao, A. Jain, T. Koschny, C. M. Soukoulis, Electromagnetically induced transparency and absorption in metamaterials: The radiating

- two-oscillator model and its experimental confirmation., *Physical Review Letters* 109 (18) (2012) 187401.
- [18] A. Artar, A. A. Yanik, H. Altug, Multispectral plasmon induced transparency in coupled meta-atoms., *Nano Letters* 11 (4) (2011) 1685–1689.
- [19] A. E. Cetin, A. Artar, M. Turkmen, A. A. Yanik, H. Altug, Plasmon induced transparency in cascaded p-shaped metamaterials., *Optics Express* 19 (23) (2011) 22607–22618.
- [20] U. Hohenester, A. Trugler, Mnpbem - a matlab toolbox for the simulation of plasmonic nanoparticles., *Computer Physics Communications* 183 (2) (2012) 370–381.
- [21] S. Coskun, B. Aksoy, H. E. Unalan, Polyol synthesis of silver nanowires: An extensive parametric study., *Crystal Growth and Design* 11 (11) (2011) 4963–4969.
- [22] B. J. Wiley, Y. Xiong, Y. Xia, Z. Y. Li, Y. Yin, Right bipyramids of silver: A new shape derived from single twinned seeds., *Nano Letters* 6 (4) (2006) 765–768.